

Li(2p←2s)+Na(3s) pressure broadening in thefar-wing and line-core profiles

F Talbi, N Lamoudi, L Reggami, M T Bouazza, K Alioua, and M Bouledroua

Citation: Chin. Phys. B, 2022, 31 (**7**): 073401. DOI: 10.1088/1674-1056/ac43a0
Journal homepage: http://cpb.iphy.ac.cn; http://iopscience.iop.org/cpb

What follows is a list of articles you may be interested in

Oscillator strength study of the excitations of valence-shell of C_2H_2 by high-resolution inelastic x-ray scattering

Qiang Sun(孙强), Ya-Wei Liu(刘亚伟), Yuan-Chen Xu(徐远琛), Li-Han Wang(王礼涵), Tian-Jun Li(李天钧), Shu-Xing Wang(汪书兴), Ke Yang(杨科), and Lin-Fan Zhu(朱林繁)
Chin. Phys. B, 2022, 31 (**5**): 053401. DOI: 10.1088/1674-1056/ac422e

Charge transfer in low-energy collisions ofBe^{3+} and B^{4+} ions with He

Kun Wang(王堃), Yi-Zhi Qu(屈一至), Chun-Hua Liu(刘春华), Ling Liu(刘玲), Yong Wu(吴勇), H P Liebermann, Robert J. Buenker
Chin. Phys. B, 2020, 29 (**9**): 093401. DOI: 10.1088/1674-1056/aba276

Isotope effect and Coriolis coupling effect forthe Li + H(D)Cl→LiCl + H(D) reaction

Hongsheng Zhai(翟红生), Guanglei Liang(梁广雷), Junxia Ding(丁俊霞), Yufang Liu(刘玉芳)
Chin. Phys. B, 2019, 28 (**5**): 053401. DOI: 10.1088/1674-1056/28/5/053401

Collision of cold CaF molecules: Towards evaporative cooling

Yuefeng Gu(顾跃凤), Yunxia Huang(黄云霞), Chuanliang Li(李传亮), Xiaohua Yang(杨晓华)
Chin. Phys. B, 2019, 28 (**3**): 033401. DOI: 10.1088/1674-1056/28/3/033401

Solvent effects and potential of mean force study of the S_N2 reaction of CH_3F+CN^- in water

Chen Li(李琛), Peng Liu(刘鹏), Yongfang Li(李永方), Dunyou Wang(王敦友)
Chin. Phys. B, 2018, 27 (**3**): 033401. DOI: 10.1088/1674-1056/27/3/033401

Li (2p ← 2s) + Na (3s) pressure broadening in the far-wing and line-core profiles

F Talbi[1,2], N Lamoudi[1,3], L Reggami[1], M T Bouazza[1,4,†], K Alioua[5], and M Bouledroua[2]

[1] *Physics Department, Badji Mokhtar University, B.P.* 12, *Annaba* 23000, *Algeria*
[2] *Laboratoire de Physique des Rayonnements, Badji Mokhtar University, B.P.* 12, *Annaba* 23000, *Algeria*
[3] *Laboratoire d'Etude des Surfaces et Interfaces de la Matière Solide (LESIMS), Badji Mokhtar University, B.P.*12 *Annaba* 23000, *Algeria*
[4] *Laboratoire LAMA, Laboratoire des Matériaux Avancés (LAMA), Badji Mokhtar University, B.P.*12 *Annaba* 23000, *Algeria*
[5] *Laboratoire de Physique de la Matière et du Rayonnement LPMR, Université Chérif Messaidia, B. P.* 1553, *Souk-Ahras* 41000, *Algeria*

(Received 13 September 2021; revised manuscript received 26 November 2021; accepted manuscript online 16 December 2021)

This work reports pressure-broadening line-wing and line-core of the lithium Li (2p ← 2s) resonance line perturbed by ground sodium Na (3s) atoms. In far-wing regions, the calculations are performed quantum-mechanically and are intended to examine the photoabsorption coefficients at diverse temperatures. The results show the existence of three satellites, in the blue wing near the wavelengths 470 nm and in the red wing around 862 nm and 1070 nm. For the line-core region, by adopting the simplified Baranger model, the line-width and line-shift rates are determined, and their variation law with temperature is examined. No published data were found to compare these results with.

Keywords: pressure broadening, line-core broadening, far-wing spectra, photoabsorption

PACS: 34.20.–b, 52.25.Os, 31.50.Df, 95.30.Ky **DOI:** 10.1088/1674-1056/ac43a0

1. Introduction

The investigations on the line core and the far wings of molecular spectral profiles have been lately become a subject of great interest in astrophysics, spectroscopy, quantum chemistry and laser physics. In fact, the interpretations of the collisional broadened line profiles of alkali-metal atoms allow us to investigate the interstellar mediums, because several observations demonstrate that the environment of astronomical objects are primary dominated by the alkali-metal atoms.[1–3] Due to this high importance, a large number of experimentalists and theoreticians have long been interested in studying the spectral line broadening in the core and in the far wings caused by the interaction of alkali-metal atoms with atoms of their surrounding environment. The theoretical studies have employed semi-classical[4–6] and quantum[7–12] models. Over the last few years, our group has simulate quantum-mechanically the photoabsorption spectra of alkali-metal atoms broadened by collision with like, unlike or rare-gas atoms. In our recent paper,[13] we have carried out the absorption spectra of a radiating sodium atoms Na (3p ← 3s) perturbed by ground lithium Li (2s) atoms. The current paper is concerned with the quantal study of pressure-broadening phenomena which affects the Li (2p ← 2s) resonance line in the wings and core when the lithium atoms are interacting with ground sodium Na (3s) atoms. In the next section we will describe the method used to construct the required potential-energy curves and the transition dipole moments. In Section 3, we will use them to carry out the radiative lifetime of the ro-vibrational levels of the excited molecular states. In Section 4, we will calculate the diffusion coefficients of ground Li(2s) and excited Li (2p) lithium atoms in sodium gas to see how accurate the LiNa potentials are. Section 5 is divided into two subsections, Subsection 5.1 is devoted to the computation of the reduced-absorption coefficients; this part is more concerned with the designation of satellite peak positions and origins in the blue and red wings. In Subsection 5.2, the width and shift of line-core will be evaluated and their variation laws with temperature will be examined.

Unless otherwise stated, atomic units (a.u.) are used all over this paper; in particular, energies are in Hartrees (E_h), distances in Bohrs (a_0), and $\hbar = 1$.

2. Potential and dipole moments constructions

The quantum-mechanical investigation of the line broadening in the core or in the wings of the lithium Li (2p ← 2s) spectra, perturbed by ground sodium atoms, needs to be started by the determination of the potential-energy curves along which the dimers Li (2s) + Na (3s) and Li (2p) + Na (3s) interact. More precisely, this section is devoted to the construction of the singlet $X^1\Sigma^+$ and triplet $a^3\Sigma^+$ potential-energy curves via which Li (2s) interacts with Na (3s) and of the singlet $A^1\Sigma^+$ and $B^1\Pi$ and the triplet $b^3\Pi$ and $c^3\Sigma^+$ potential curves via which Li (2p) interacts with Na (3s).

To this aim, we adopted the *ab initio* data points generated by Aubert–Frécon M,[14] which we extended smoothly to the Born–Mayer potential[15] $V(R) \sim \alpha \exp(-\beta R)$, in the short-

†Corresponding author. E-mail: taharbouazza@yahoo.com
© 2022 Chinese Physical Society and IOP Publishing Ltd

range internuclear distances R, and to the well-known form $V(R) \sim -\sum_n C_n R^{-n}$, in the long-range distances. In these formulas, α and β are two constant parameters and C_n, with $n = 6$, 8, and 10, are the dispersion coefficients adopted from Marinescu and Sadeghpour.[16] All these constants are listed in Table 1.

Table 1. Adopted short- and long-range parameters (in a.u.) for the construction of ground Li(2s) + Na(3s) and excited Li(2p) + Na(3s) potential-energy curves. All the dispersion coefficients are from Marinescu and Sadeghpour.[16] Numbers in square brackets represent powers of ten: $[m] = 10^{+m}$.

LiNa	Short ranges		Long ranges		
molecular states	α	β	C_6	C_8	C_{10}
$X^1\Sigma^+$	47.88	2.228	1.4594 [3]	9.8060 [4]	9.1279 [6]
$A^1\Sigma^+$	8.195	1.504	1.6829 [4]	6.9559 [5]	–
$B^1\Pi$	2.758	1.127	5.1409 [3]	9.5887 [4]	–
$a^3\Sigma^+$	1.625	0.872	1.4594 [3]	9.8060 [4]	9.1279 [6]
$b^3\Pi$	5.209 [4]	4.675	5.1409 [3]	9.5887 [4]	–
$c^3\Sigma^+$	4.111	1.176	1.6829 [4]	6.9559 [5]	–

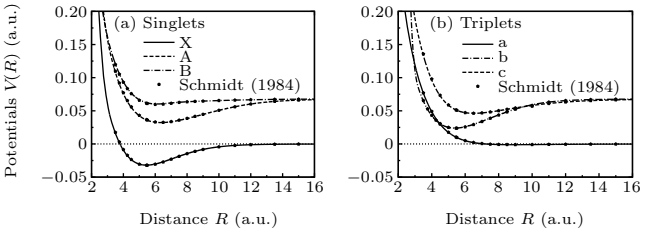


Fig. 1. Li(2s) + Na(3s) and Li(2p) + Na(3s) potential-energy curves $V(R)$ variation with the internuclear distance R. All singlet and triplet curves are compared with theoretical data from Ref. [17].

Figure 1 shows the constructed potential curves relative to the singlet and triplet LiNa molecular states. Some of the theoretical data points of Schmidt–Mink *et al.*[17] are also presented for comparison. Mabrouk and Berriche[18] determined the energy difference 0.0679 between both 2s–3s and 2p–3s asymptotic dissociation limits, which is identical to the experimental value cited in Ref. [18]. This energy turns to be very close to 0.0680 computed by Aubert–Frécon.[14] The corresponding spectroscopic data derived from the present curves, namely, the equilibrium distance R_e, the dissociation energy D_e, and the minimum-to-minimum electronic excitation energy T_e, are given and compared with some theoretical[17–20] and measured values[21–23] in Table 2. To further verify the accuracy of the constructed potentials, we have determined their rotational-vibrational energy levels and compared them with the corresponding available published data. Tables 3 and 4 display, for a few number of vibrational quantum number v, the rotational-vibrational energy levels $-E(v,J)$, with $J = 0$ for Σ states and $J = 1$ for Π states.

Table 2. Spectroscopic constants related to the ground and excited LiNa dimer. They are compared with some published results.

Molecular states	R_e (Å)	D_e (cm^{-1})	T_e (cm^{-1})	Ref.
$X^1\Sigma^+$	2.882	7006	–	this work
	2.890	7057	–	[17][a]
	2.873	7054	–	[18][a]
	2.889	7033	–	[19][a]
	2.895	7117	–	[20][a]
	2.885	7068	–	[22][b]
	2.889	7103.5 ± 0.1	–	[21][b]
$A^1\Sigma^+$	3.366	7844	14066	this work
	3.371	7795	14200	[17][a]
	3.360	7859	14101	[18][a]
	–	7776	14196	[23][b]
$B^1\Pi$	3.239	1688	20221	this work
	3.220	1865	20130	[17][a]
	3.228	1721	20239	[18][a]
	3.119	1910	20062	[22][b]
$a^3\Sigma^+$	4.720	238	6768	this work
	4.754	216	6841	[17][a]
	4.720	220	6834	[18][a]
$b^3\Pi$	2.847	9676	12234	this work
	2.858	9720	12275	[17][a]
	2.841	9704	12255	[18][a]
$c^3\Sigma^+$	3.450	4779	17131	this work
	3.449	4793	17202	[17][a]
	3.440	4799	17160	[18][a]

[a]Theoretical, [b]Experimental.

Table 3. Rotationless-vibrational energy levels $-E(v,J)$, in cm^{-1}, of the singlet LiNa molecular states.

Vibrational level	$X^1\Sigma^+$			$A^1\Sigma^+$		$B^1\Pi$		
v	$-E(v,J=0)$	[17]	[22]	$-E(v,J=0)$	[17]	$-E(v,J=1)$	[17]	[22]
0	126.31	128	128.1	93.78	94	85.47	90	103.4
1	376.76	381	351.7	279.94	280	250.83	265	273.7
2	624.07	632	632.0	464.28	465	405.37	431	466.0
7	1811.30	1832	1831.9	1359.21	1360	955.13	1059	1098.6
12	2912.68	2945	2942.9	2210.09	2209	1272.59	1404	1463.4
17	3920.66	3961	3959.7	3017.32	3013	–	–	–
20	4476.20	4520	4521.1	3480.64	3474	1587.42	1746	–
24	5152.90	5201	5206.6	4073.50	4064	1661.08	1832	–
30	6009.56	–	6078.1	4907.42	–	–	–	–
43	6978.26	–	6452.27	–	–	–	–	–
73	–	–	7844.30	–	–	–	–	–

Table 4. Rotationless-vibrational energy levels $-E(v,J)$, in cm^{-1}, of the triplet LiNa molecular states.

Vibrational level	$a^3\Sigma^+$		$b^3\Pi$		$c^3\Sigma^+$	
v	$-E(v,J=0)$	[17]	$-E(v,J=1)$	[17]	$-E(v,J=0)$	[17]
0	20.43	20	85.22	86	124.05	125
1	58.50	56	253.53	225	371.34	373
2	92.84	89	419.04	422	616.34	619
3	123.41	119	581.73	585	858.97	863
4	150.15	144	741.62	746	1099.31	1104
5	172.93	166	898.71	903	1337.33	1343
10	231.58	–	1642.11	1684	2492.62	2502
12	237.63	–	1919.70	1925	2938.37	2950
22	–	–	3132.63	3137	5022.11	5038
56	–	–	4778.81	–	9551.75	–
65	–	–	–	–	9675.41	–

We also need to know in the following calculations the transition dipole moments $D(R)$ (TDMs) correlated with the allowed molecular transitions among the singlet $A^1\Sigma^+ \leftarrow X^1\Sigma^+$ and $B^1\Pi \leftarrow X^1\Sigma^+$ and the triplet $b^3\Pi \leftarrow a^3\Sigma^+$ and $c^3\Sigma^+ \leftarrow a^3\Sigma^+$ states. In the present constructions we utilize the data points generated by Aubert–Frécon M,[14] which we connected in small distances to a linear form and for large distances R to $D(R) \sim D_\infty + AR^{-3}$, proposed by Chu and Dalgarno.[24] Here, $D_\infty \simeq 2.359$ is the atomic dipole moment obtained as $R \to \infty$, and the calculations yield $A = +3474.61$ and $A = -1668.11$ for the $\Sigma\Sigma$ and $\Sigma\Pi$ transitions, respectively. The TDM curves are shown in Fig. 2, where the X–A dipole moments are compared with *ab-initio* data points from Mabrouk and Berriche.[18]

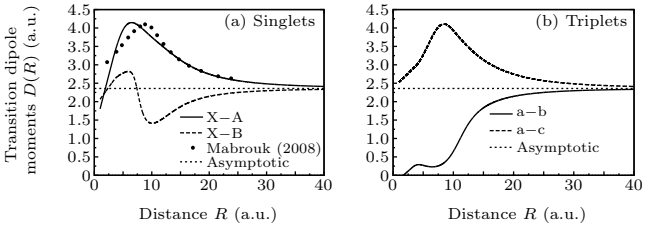


Fig. 2. Transition dipole moments as a function of internuclear R. The singlet X–A moments are compared with theoretical data from Ref. [18].

3. Radiative lifetimes

We propose in this section to calculate with our constructed potentials and transition dipole moments the radiative lifetimes of the ro-vibrational levels of the excited LiNa molecular states.

The radiative lifetime $\tau = 1/\mathcal{A}(v'J\Lambda')$ of an upper rotational-vibrational molecular state $(v'J\Lambda')$ is defined in quantum mechanics as the inverse of the sum of the probabilities[11,25]

$$\mathcal{A}(v'J\Lambda') = \frac{64\pi^4}{3hc^3}\frac{2-\delta_{0,\Lambda'+\Lambda''}}{2-\delta_{0,\Lambda'}} \times \left[\int_0^\infty \nu^3 \left|\mathcal{M}_{v'J\Lambda'\mapsto\varepsilon''J\Lambda''}\right|^2 \mathrm{d}\varepsilon'' + \sum_{v''} \nu^3 \left|\mathcal{M}_{v'J\Lambda'\mapsto v''J\Lambda''}\right|^2\right] \quad (1)$$

of the spontaneous bound–free and bound–bound emissions. In this equation, $\mathcal{M}_{\xi'\mapsto\xi''} = \langle\psi_{\xi'}|D(R)|\psi_{\xi''}\rangle$ are the dipole matrix elements associated with the transitions from the upper bound levels $\xi' = (v'J\Lambda')$ to the lower bound levels $\xi'' = (v''J\Lambda'')$ and continuum $\xi'' = (\varepsilon''J\Lambda'')$, $h = 2\pi\hbar$ is the Planck's constant, c is the speed of light, and ν is the $\xi' \mapsto \xi''$ transition frequency. The bound and free wave functions $\psi_\xi(R)$ are solutions of the radial wave equation

$$\frac{\mathrm{d}^2\psi_\xi(R)}{\mathrm{d}R^2} + \frac{2\mu}{\hbar^2}\left[\varepsilon - V(R) - \frac{\hbar^2}{2\mu}\frac{J(J+1)-\Lambda^2}{R^2}\right]\psi_\xi(R) = 0, \quad (2)$$

with Λ being the projection of the orbital angular momentum on the internuclear axis.[25] The free states are associated with the energy-normalized wave functions, while the bound states are space-normalized wave functions.

The obtained lifetime results of a few rotational-vibrational levels, relative to the singlet $A^1\Sigma^+$ and $B^1\Pi$ and to the triplet $b^3\Sigma^+$ and $c^3\Pi$ states, are compiled in Table 5. In addition, by considering in the vicinity of the dissociation limits the highest rotationless-vibrational states, it is possible to determine the atomic radiative lifetime τ_a for Li(2p) excited state. This can be done by averaging the four lifetimes that correspond to the highest rotationless vibrational levels, shown in bold in Table 5. In such a case, the atomic lifetime τ_a is related to the statistically weighted sum of $\mathcal{A}(v'J\Lambda')$ with

$$\frac{1}{\tau_a} = \frac{1}{12}\mathcal{A}(v'_{\max}00) + \frac{2}{12}\mathcal{A}(v'_{\max}01) + \frac{3}{12}\mathcal{A}(v00) + \frac{6}{12}\mathcal{A}(v'_{\max}01). \quad (3)$$

The present theoretical calculations yield the radiative lifetime 27.16 ns for the 2p lithium state. The deduced value is consistent with the experimentally determined values 27.1018(14) ns of Le Roy *et al.*,[26] 27.09(4) ns of Schmitt *et al.*,[27] 27.11(6) ns of Volz and Schmoranzer,[28] and 27.22(20) ns of Carlsson and Sturesson.[29] McAlexander *et al.* deduced from their experiments the values 26.99(16) ns for the ^{7}Li($2p^2P^\circ$) state,[31] and 27.102(2) ns,

for the ^{7}Li($2p^2P^\circ_{1/2}$) state.[31] The NIST recommended value is 27.11 ns.[32]

In all cases, the above comparisons show minute discrepancies with published works, which lead us to fully trust in our constructed LiNa potentials and TDMs.

Table 5. LiNa radiative lifetimes (in ns) of the singlet, $A^1\Sigma^+$ and $B^1\Pi$, and triplet, $b^3\Sigma^+$ and $c^3\Pi$, states.

Level	J						
v	0	1	10	20	30	40	50
				$A^1\Sigma^+$			
0	12.53	–	12.56	12.64	12.76	12.93	13.16
10	55.93	–	54.04	50.57	47.58	44.48	43.68
20	59.66	–	57.65	53.83	49.79	44.63	37.87
30	47.29	–	45.28	41.03	34.52	30.20	23.25
40	41.13	–	38.39	31.57	24.61	16.97	16.09
50	37.57	–	31.29	20.34	15.90	15.88	15.97
60	35.77	–	18.69	16.96	17.20	17.55	18.38
70	23.52	–	23.48	–	–	–	–
73	**26.73**	–	–	–	–	–	–
				$B^1\Pi$			
0	–	8.26	8.27	8.33	–	–	–
5	–	54.04	14.29	15.12	–	–	–
10	–	103.15	29.77	31.03	–	–	–
15	–	103.15	39.69	40.6	–	–	–
20	–	141.47	42.07	41.78	–	–	–
25	–	58.91	34.73	32.38	–	–	–
29	–	**27.91**	–	–	–	–	–
				$b^3\Pi$			
60	–	77.43	40.50	37.10	–	–	–
65	–	**27.59**	–	–	–	–	–
				$c^3\Sigma^+$			
0	37.29	–	37.17	36.86	36.34	35.63	34.73
10	61.26	–	56.07	53.88	47.69	41.70	34.17
20	47.19	–	42.61	40.83	35.03	22.81	19.77
30	39.83	–	33.38	30.87	22.04	17.34	16.95
40	37.00	–	25.63	18.49	17.03	17.01	17.22
50	27.68	–	20.06	20.56	22.0	–	–
56	**25.75**	–	–	–	–	–	–

4. Diffusion properties

We have also suggested, to assess the potential-energy curves constructed above, to look at the diffusion of ground Li(2s) and excited Li(2p) atoms into a dilute gas made of sodium atoms. The temperature-dependent diffusion coefficient $D(T)$ for dilute gas is calculated by using the Chapman–Enskog method.[33] For one temperature T and atomic density n, this coefficient is given by

$$D(T) = \frac{3}{8n}\sqrt{\frac{\pi k_B T}{2\mu}}\frac{1}{\Omega^{(1,1)}(T)}, \tag{4}$$

where k_B is Boltzmann's constant, μ is the reduced mass of the two colliding atoms, and $\Omega^{(1,1)}(T)$ is the collision integral defined as

$$\Omega^{(1,1)}(T) = \frac{1}{2(k_B T)^3}\int_0^\infty E^2 Q_D(E)\exp\left(-\frac{E}{k_B T}\right)\mathrm{d}E, \tag{5}$$

with $Q_D(E)$ being the quantum-mechanical effective cross section in diffusion

$$Q_D = \frac{4\pi}{k^2}\sum_{l=0}^{\infty}(l+1)\sin^2(\eta_{l+1}-\eta_l), \tag{6}$$

where $k = (2\mu E)^{1/2}$ is the wave number and η_l is the phase shift obtained by solving the corresponding radial wave Eq. (2). For the diffusion of the ground Li(2s) atom in sodium gas, the diffusion cross section is given by the average

$$Q_D(E) = \frac{1}{4}Q_D\left(X^1\Sigma^+\right) + \frac{3}{4}Q_D\left(a^3\Sigma^+\right), \tag{7}$$

and by the following average:

$$Q_D(E) = \frac{1}{4}\left[\frac{1}{3}Q_D\left(A^1\Sigma^+\right) + \frac{2}{3}Q_D\left(B^1\Pi\right)\right] + \frac{3}{4}\left[\frac{1}{3}Q_D\left(b^3\Sigma^+\right) + \frac{2}{3}Q_D\left(c^3\Pi\right)\right]. \tag{8}$$

for the diffusion cross section of the excited Li(2p) in sodium gas.

The diffusion coefficients in the temperature range 100 K–2000 K at gas pressure $p = 1$ atm are listed in Table 6 for ground and excited states. To our knowledge, no published results are available for the LiNa system, so our results may serve as a prediction for future works.

Table 6. Diffusion coefficients $D(T)$ for ground Li(2s) and excited Li(2p) in Na(3s) at several temperatures.

Temperature	D ($m^2 \cdot s^{-1}$)	
T (K)	Li(2s) in Na(3s)	Li(2p) in Na(3s)
100	0.013	0.008
200	0.058	0.026
500	0.422	0.148
1000	1.810	0.793
1500	4.400	2.730
2000	8.920	7.276

5. Far-wing and line-core pressure broadening

In the remaining sections, we are interested in the pressure broadening phenomena that a lithium atom absorbing a photon undergoes while it interacts with a ground sodium atom. The Li($2p \leftarrow 2s$) photoabsorption is practically examined when the absorbing atom is moving into a dilute sodium gas at a fixed temperature T. In such a case, the natural spectrum is physically affected in its line core and its far wings. Thus, the aim of this work is twofold: (i) to determine quantum mechanically the far-wing absorption profiles of the absorbing atom, and (ii) to quantify the amount of broadening of the $2p \leftarrow 2s$ line and its displacement from the unperturbed wavelength $\lambda_0 \simeq 670.8$ nm.

5.1. Far-wing spectra

The collisional broadening phenomenon has been reviewed by Allard and Kielkopf[34] and Szudy and Baylis.[35] However, the far-wing pressure broadening process is quantified in molecular spectroscopy by means of the reduced absorption coefficients. The main relationships for these coefficients are given in Refs. [12,36].

For the case of the LiNa quasi molecule, the total reduced absorption coefficient is the sum of contribution corresponding to the four allowed transitions $A^1\Sigma^+ \leftarrow X^1\Sigma^+$, $B^1\Pi \leftarrow X^1\Sigma^+$, $b^3\Pi \leftarrow a^3\Sigma^+$, and $c^3\Sigma^+ \leftarrow a^3\Sigma^+$. Usually, for an allowed molecular transition, the photoabsorption coefficient is the sum of four absorption coefficients corresponding to four possible transitions, namely, bound–bound (b–b), bound–free (b–f), free–bound (f–b), and free–free (f–f). The equations which give different reduced absorption coefficients relating to each type of transition are given by the following expressions:

For (b–b) transition,

$$k_{\mathrm{r}}^{\mathrm{b\text{–}b}}(\nu,T) = \frac{8\pi^3\nu}{3hc}\varpi\left[\frac{2\pi\hbar^2}{\mu k_{\mathrm{B}}T}\right]^{3/2}\sum_{v''J}\sum_{v'} g(\nu-\nu_{\mathrm{tr}})(2J+1) \times\mathcal{M}^2_{v''J\Lambda''\mapsto v'J\Lambda'}\exp\left(-\frac{E_{v''J\Lambda''}}{k_{\mathrm{B}}T}\right), \tag{9}$$

where ϖ is the probability the lithium and sodium atoms form a molecule in the lower electronic state defined as

$$\varpi = \frac{2-\delta_{0,\Lambda'+\Lambda''}}{2-\delta_{0,\Lambda''}}\frac{2S_{\mathrm{LiNa}}+1}{(2S_{\mathrm{Li}}+1)(2S_{\mathrm{Na}}+1)}. \tag{10}$$

For (b–f) transition,

$$k_{\mathrm{r}}^{\mathrm{b\text{–}f}}(\nu,T) = \frac{8\pi^3\nu}{3hc}\varpi\left[\frac{2\pi\hbar^2}{\mu k_{\mathrm{B}}T}\right]^{3/2}\sum_{v''J}(2J+1) \times\mathcal{M}^2_{v''J\Lambda''\mapsto\varepsilon'J\Lambda'}\exp\left(-\frac{E_{v''J\Lambda''}}{k_{\mathrm{B}}T}\right). \tag{11}$$

For (f–b) transition,

$$k_{\mathrm{r}}^{\mathrm{f\text{-}b}}(\nu,T) = \frac{8\pi^3\nu}{3hc}\varpi\left[\frac{2\pi\hbar^2}{\mu k_{\mathrm{B}}T}\right]^{3/2}\sum_{v'J}(2J+1) \times\mathcal{M}^2_{\varepsilon''J\Lambda''\mapsto v'J\Lambda'}\exp\left(-\frac{\varepsilon''}{k_{\mathrm{B}}T}\right). \tag{12}$$

For (f–f) transition,

$$k_{\mathrm{r}}^{\mathrm{f\text{-}f}}(\nu,T) = \frac{8\pi^3\nu}{3hc}\varpi\left[\frac{2\pi\hbar^2}{\mu k_{\mathrm{B}}T}\right]^{3/2}\sum_{J}\int \mathrm{d}\varepsilon'(2J+1) \times\mathcal{M}^2_{\varepsilon''J\Lambda''\mapsto\varepsilon'J\Lambda'}\exp\left(-\frac{\varepsilon''}{k_{\mathrm{B}}T}\right). \tag{13}$$

The bound and free wave functions, which occur in the dipole matrix elements $\mathcal{M}_{\xi''\mapsto\xi'}$ of Eqs. (9) and (11)–(13), are normalized in the same way described in Section 3 above.

Figure 3 illustrates our results of simulation of the reduced photoabsorption coefficients corresponding to LiNa system carried out with our full quantum-mechanical calculations, at the temperature $T = 2000$ K for wavelengths ranging from 400 nm to 1200 nm. In our computation, we have taken into account all the bound and quasibound ro-vibrational levels, and we have used a frequency step $\Delta\nu = 10\ \mathrm{cm}^{-1}$. The total spectrum represented in Fig. 3(a) shows clearly the existence of two satellites in the red wing located around 862 nm and 1070 nm. In Fig. 3(b), we display the contribution of the four partial transitions. From this curve, it is easy to see that the singlet A ← X and B ← X bands dominate the red and blue wings, respectively. Indeed, the A ← X transitions generate the 1070 nm satellite in the red wing, whereas both triplet b ← a and c ← a transitions are solely presented in the blue wing and have almost no effects on the general shape of the total spectrum. However, the b ← a transitions participate with the satellite occurring at 862 nm.

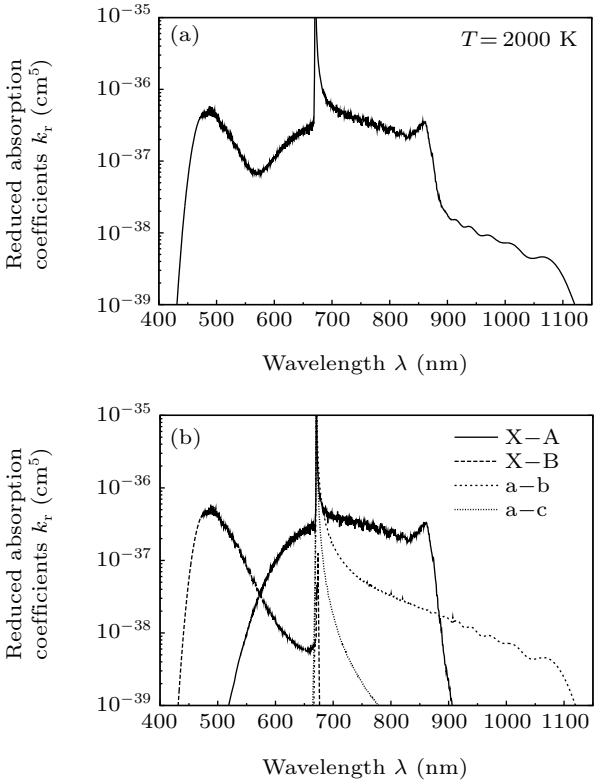


Fig. 3. LiNa photoabsorption profile at $T = 2000$ K, (a) presents the total reduced absorption coefficient, (b) displays the contribution of the four types of transition A ← X, B ← X, b ← a, and c ← a, to the total profile given in (a).

From the classical theory,[34,35] the positions of such satellites are expected to occur at wavelengths corresponding to the extrema of the potential difference curves. Hence we have plotted in Fig. 4 the potential difference $\Delta V_{\mathrm{A}\leftarrow\mathrm{X}}$, $\Delta V_{\mathrm{B}\leftarrow\mathrm{X}}$, $\Delta V_{\mathrm{b}\leftarrow\mathrm{a}}$, and $\Delta V_{\mathrm{c}\leftarrow\mathrm{a}}$ in terms of internuclear distance R. Effectively, $\Delta V_{\mathrm{A}\leftarrow\mathrm{X}}$, $\Delta V_{\mathrm{b}\leftarrow\mathrm{a}}$, and $\Delta V_{\mathrm{B}\leftarrow\mathrm{X}}$ present an extrema at R equal to 0.053 a.u., 0.041 a.u., and 0.104 a.u., respectively, corresponding to the wavelengths 868 nm, 1115 nm,

and 440 nm. The potential difference curve $\Delta V_{c\leftarrow a}$ displays no extrema. As the potential difference predicts the possible existence of satellite near the wavelength 440 nm, we represent, in Fig. 5 in arbitrary units, the modified reduced absorption coefficient $(\Delta\omega)^2 \times k_r(\Delta\omega)$, calculated at 2000 K as function of the frequency detuning $\Delta\omega = |\omega - \omega_0|$ in cm^{-1} from the lithium atomic resonance line ω_0. This modification, suggested by Lyyra *et al.*,[37] is able to highlight the weak satellites. Figure 5(a) shows the existence of a satellite for $\Delta\omega = 6310\ cm^{-1}$ in the blue wing, which corresponds to the wavelength 470 nm, close to the value predicted by the potential difference $\Delta V_{B\leftarrow X}$. Figure 5(b) confirms the existence of two satellites in the red wing, already detected.

Table 7. Satellite positions, in nm, in the blue and red wings.

Calculation method	Satellite positions	
	blue wing	red wing
Quantal	470	862 1070
Classical	440	868 1115

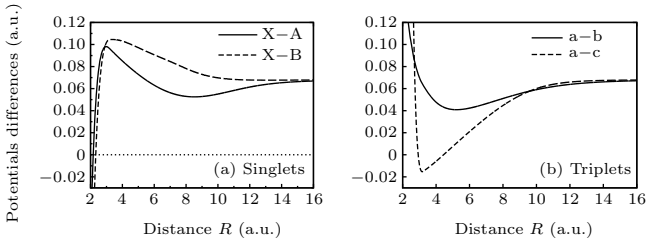


Fig. 4. The LiNa difference potentials.

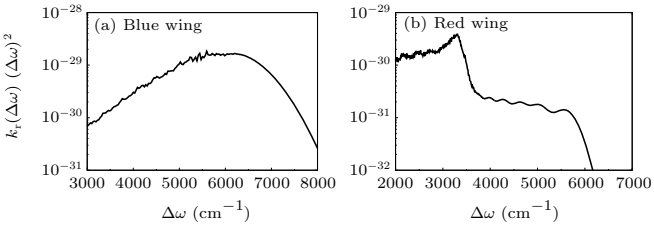


Fig. 5. Modified reduced absorption coefficient $(\Delta\omega)^2 \times k_r(\Delta\omega)$ at $T = 2000$ K as a function of detuning $\Delta\omega = |\omega - \omega_0|$.

We have also investigated the effect of temperature on the profile of the photoabsorption spectrum for temperature range 1500 K–4000 K. It is noted that the spectrum intensity decreases with increasing temperature, as shown in Fig. 6 because the spectrum is dominated by the A ← X (in the red wing) and B ← X (in the blue wing) contributions which are mainly resulted from bound-bound transitions. As T increases, the population of the lower levels decreases leading to a drastic diminution of the photoabsorption spectrum intensity. Table 7 recapitulates the three satellite positions.

Once the calculations are achieved for the line-wing profile, it is now interesting to look also at the pressure broadening phenomena in the line-core.

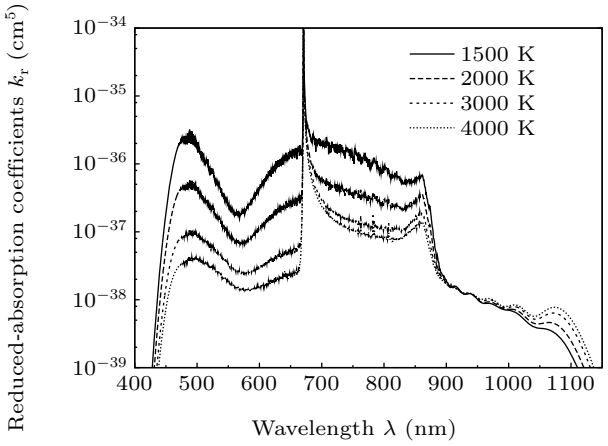


Fig. 6. Temperature effect on the shape of the photoabsorption profile. The temperatures are ranging from 1500 K to 4000 K.

5.2. Line-core pressure broadening

The atomic spectral lines are not really narrow and symmetrical, this is caused by several effects, such as natural, Doppler and pressure broadenings.[34] We are here interested in the phenomenon of pressure broadening which remains dominant in the considered temperature range.

The part of this study treats the core region of the resonance line. In other words, we attempt to calculate the full width at half maximum w and the shift s of the the lithium resonance line atom Li $(2s - 2p)$ perturbed by the sodium Na $(3s)$ atoms, where these atoms form a gas in the vicinity of emitting atoms. To accomplish this calculation, we adopted the simplified quantum mechanical model of Baranger.[38] This model treats the case where the spin-orbit effect is neglected in the range of considered temperatures.

Line-width and line-shift The line-width w and the line-shift s of Li $(2p \leftarrow 2s)$ resonnance line perturbed by Na $(3s)$ atoms are expressed by the following formula:[38]

$$w = +n\langle v \cdot Q_w \rangle_{av}, \tag{14}$$

$$s = -n\langle v \cdot Q_s \rangle_{av}, \tag{15}$$

where the minus sign in the shift means a blue or a red shift and n is the density number of the perturbing gas. The average $\langle v \cdot Q_w \rangle_{av}$ and $\langle v \cdot Q_s \rangle_{av}$ are calculated assuming the Maxwell distribution of relative velocities v. In terms of relative energy $E = (\hbar k)^2 / 2\mu$ of the colliding atoms, these expressions become

$$\langle v \cdot Q_{w,s} \rangle_{av} = \sqrt{\frac{8}{\mu\pi}} \frac{1}{(k_B T)^{3/2}} \int_0^\infty Q_{w,s}(E) \exp(-E/k_B T) E \, dE, \tag{16}$$

with Q_w and Q_s are the line-width and the line-shift cross sections, given by the sums[38]

$$Q_w = \frac{4\pi}{k^2} \sum_{l=0}^{\infty} (2l+1) \sin^2(\eta_l^{ex} - \eta_l^{gr}), \tag{17}$$

$$Q_s = \frac{\pi}{k^2}\sum_{l=0}^{\infty}(2l+1)\sin\left[2\left(\eta_l^{\rm ex}-\eta_l^{\rm gr}\right)\right]. \quad (18)$$

The elastic phase shifts $\eta_l(E)$ for each energy E and angular momentum l are determined by solving numerically the radial wave equation

$$\frac{{\rm d}^2\psi_l(R)}{{\rm d}R^2}+\left[k^2-\frac{2\mu}{\hbar^2}V(R)-\frac{l(l+1)}{R^2}\right]\psi_l(R)=0, \quad (19)$$

in which the wavefunctions $\psi_l(R)$ vary asymptotically as $R\to\infty$ like

$$\psi_l(R)\sim\sin\left(kR-\frac{1}{2}\pi+\eta_l\right). \quad (20)$$

From a statistical point of view, the total cross sections are given by the average cross sections of the singlet $Q_{w,s}^{\rm sing}$ and triplet $Q_{w,s}^{\rm trip}$ states:

$$Q_{w,s}^{\rm tot}=\frac{1}{4}Q_{w,s}^{\rm sing}+\frac{3}{4}Q_{w,s}^{\rm trip}, \quad (21)$$

which are defined by the following weighted averages[33]

$$Q_{w,s}^{\rm sing}=\frac{1}{3}Q_{\rm sing}^{\Sigma\Sigma}+\frac{2}{3}Q_{\rm sing}^{\Sigma\Pi},\quad Q_{w,s}^{\rm trip}=\frac{1}{3}\sigma_{\rm trip}^{\Sigma\Sigma}+\frac{2}{3}\sigma_{\rm trip}^{\Sigma\Pi}. \quad (22)$$

Our computed total line-width and line-shift cross sections for energies from 10^{-6} a.u. to 1 a.u. are plotted on Fig. 7.

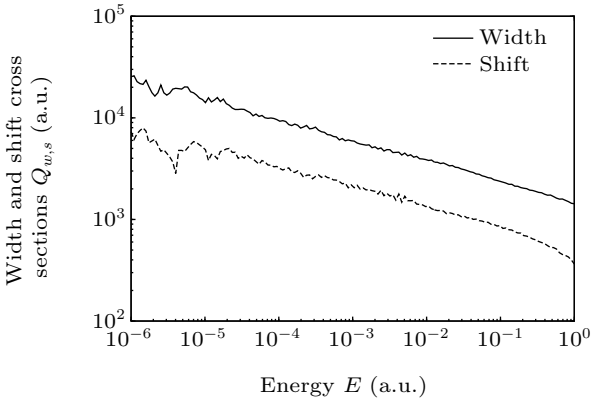


Fig. 7. Line-width and line-shift cross sections varying with energy.

Figure 8 illustrates the change of the rate coefficients w/n and s/n of the width and the shift, respectivily. We note the importance of these two coefficients at high temperature, and the same two figures show the significant divergence from the temperature T. We present also in Table 8 some values of the width and the shift rates calculated by the quantum model of Baranger.[38]

In order to find the variation law of the line-width and line-shift rates as a function of temperature T, we fit correctly the computed results of these rates to the mathematical expression of the form $\sim\alpha T^{\beta}$ with α and β being constant parameters. Their values are listed in Table 9. Representations of the width and shift rates in termsof temperature T are made on the same Fig. 8.

Table 8. The width and shift rate values at different temperatures.

Temperature	w/n	s/n
T (K)	(10^{-8} cm^3·s^{-1})	
100	+1.222	−0.438
500	+1.986	−0.724
1000	+2.479	−0.890
3000	+3.514	−1.221
5000	+4.096	−1.423
10000	+4.992	−1.752

Table 9. Fitting parameters of the width and shift rate coefficients as they appear in $\sim\alpha T^{\beta}$.

Rate	Parameters	
coefficient	α	β
Width	0.456 ± 0.004	0.316 ± 0.001
Shift	0.187 ± 0.002	0.296 ± 0.002

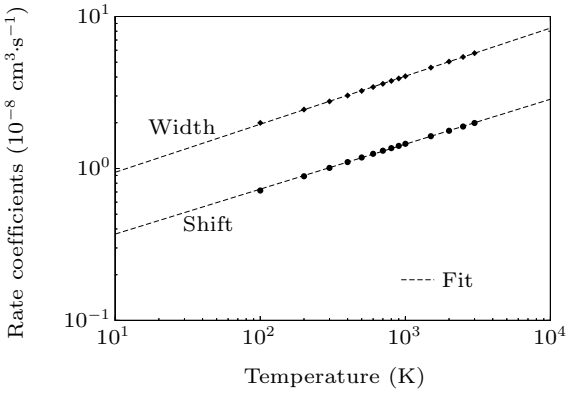


Fig. 8. Width and shift rate coefficents w/n and $-s/n$ as a function of temperature.

6. Conclusion

In this paper, we have primarily constructed the LiNa ground and excited interatomic potential curves as well as the transition dipole moments that connected them. To evaluate the reliability of our constructions, the rotational vibrational energy levels, the radiative lifetimes of excited states, and the diffusion coefficients have been carried out. We have then performed full quantum-mechanical calculation to simulate the Li$(2{\rm p}\leftarrow 2{\rm s})$ + Na$(3{\rm s})$ absorption profile spectra and to determine the line-width and line-shift parameters. The results demonstrate the sensitivity of the far wing profiles on temperature and the appearance of two red satellite peaks located around the wavelength 862 nm and 1070 nm. However, the blue satellite predicted by the potential difference close to 440 nm has been detected by means to the modification already suggested by Lyyra *et al.*[37] which is able to highlight the weak satellite.

Acknowledgments

This work has been realized within the framework of the PNR project 8/423/4388. The authors acknowledge support

from the Algerian Ministry of Higher Education and ANDRU.

References

[1] Hawley S L 2001 *Proceedings of the* 12*th Cambridge Workshop on cool Stars, Stellar Systems, and the Sun*, July 30–August 3, 2001 (University of Colorado USA) p. 97

[2] Allard N F, Allard F, Hauschildt P H, Kielkopf J F and Machin L 2003 *Astronomy & Astrophysics* **411** L473

[3] Allard N F, Allard F and Kielkopf J F 2005 *Astronomy & Astrophysics* **440** 1195

[4] Blank L and Weeks D E 2014 *Phys. Rev. A* **90** 022510

[5] Allard N F 2014 *Advances in Space Research* **54** 1285

[6] Allard N F, Nakayama A, Stienkemeier F, Kielkopf J F, Guillon G and Viel A 2014 *Advances in Space Research* **54** 1290

[7] Zhu C, Babb J F and Dalgarno A 2005 *Phys. Rev. A* **71** 052710

[8] Zhu C, Babb J F and Dalgarno A 2006 *Phys. Rev. A* **73** 012506

[9] Boutarfa H, Alioua K, Bouledroua M, Allouche A R and Aubert-Frécon M 2012 *Phys. Rev. A* **86** 052504

[10] Buchoucha S, Alioua K and Bouledroua M 2017 *Chin. Phys. B* **26** 073202

[11] Lamoudi N, Bouledroua M, Alioua K, Allouche A R and Aubert-Frécon M 2013 *Phys. Rev. A* **87** 52713

[12] Talbi F, Bouledroua M and Alioua K 2008 *Eur. Phys. J D* **50** 141

[13] Lamoudi N, Talbi F, Bouazza M T, Bouledroua M and Alioua K 2019 *Chin. Phys. B* **28** 063202

[14] Aubert-Frécon M *Private Communication*

[15] Pauly H 1979 *Atomi-Molecule Collision Theory*, Bernstein R B Edn. (New York: Plenum press)

[16] Marinescu M and Sadeghpour R H 1999 *Phys. Rev. A* **59** 390

[17] Schmidt-Mink I, Müller W and Meyer W 1984 *Chem. Phys. Lett.* **112** 120

[18] Mabrouk N and Berriche H 2008 *J. Phys. B* **41** 155101

[19] Müller W and Meyer W 1984 *J. Chem. Phys* **80** 3311

[20] Fedorov D A, Derevianko A and Varganov S A 2014 *J. Chem. Phys* **140** 184315

[21] Steinke M, Knöckel H and Tiemann E 2012 *Phys. Rev. A* **85** 042720

[22] Engelke F, Ennen G and Meiwes K H 1982 *Chem. Phys* **66** 391

[23] Kappes M M, Marti K O, Radi P, Schär M and Schumacher E 1984 *Chem. Phys. Lett.* **107** 6

[24] Chu X and Dalgarno A 2002 *Phys. Rev. A* **66** 024701

[25] Demtröder W 2006 *Atoms, Molecules and Photons* (Berlin Heidelberg: Springer-Verlag)

[26] Le Roy R J, Dattani N S, Coxon J A, Ross A J, Crozet P and Linton C 2009 *J. Chem. Phys* **131** 204309

[27] Schmitt A, Volz U and Schmoranzer H 1997 *Proceedings of ICAMDATA* (Maryland: Gaithersburg)

[28] Volz U and Schmoranzer H 1996 *Phys. Scr. T* **T65** 48

[29] Carlsson J and Sturesson L 1989 *Z. Phys. D* **14** 281

[30] McAlexander W I, Abraham E R I, Ritchie N W M, Williams C J, Stoof H T C and Hulet R G 1995 *Phys. Rev. A* **51** R871

[31] McAlexander W I, Abraham E R I and Hulet R G 1996 *Phys. Rev. A* **54** R5

[32] Kramida A, Ralchenko Y, Reader J and NIST ASD Team 2014 *NIST Atomic Spectra Database* (ver. 5.2), [Online]. [2015, April 21]. National Institute of Standards and Technology, Gaithersburg, MD.

[33] Mason E A and McDaniel E W 1988 *Transport Properties of Ions in Gases* (New York: Wiley and Sons, Inc.)

[34] Allard N F and Kielkopf J F 1982 *Rev. Mod.* **54** 1103

[35] Szudy J and Baylis W E 1996 *Phys. Rep.* **266** 127

[36] Chung H K, Kirby K and Babb J F 2001 *Phys. Rev. A* **63** 032516

[37] Lyyra A M, Sando K M and Kleiber P D 1987 *Phys. Rev. A* **35** 915

[38] Baranger M 1958 *Phys. Rev.* **111** 481